Adsorption (2011) 17: 273–283
DOI 10.1007/s10450-011-9323-9

Novel adsorbent hollow fibres for oxygen concentration

J.M. Nevell · S.P. Perera

Received: 15 May 2010 / Accepted: 10 January 2011 / Published online: 27 January 2011

Abstract The research examined the development of adsorbent hollow fibres as a low pressure drop structure for the production of oxygen-enriched air. The potential benefits of using a low pressure drop flexible adsorbent structure with molecular sieving properties over a bed packed with pellets include a low attrition resistance which could extend the life of the adsorbent structure. Highly macroporous, highly adsorbent loaded (up to 90 wt%) fibres were produced. By increasing adsorbent density, the separative performance and nitrogen loading were improved. The separative performance of the adsorbent fibre was found to be slightly inferior to that of the bed of smaller 0.4–0.8 mm beads, as the diffusion path length was longer in the fibres and caused increased mass transfer resistances within the macroporous structure. The pressure drop through the fibre was found to be 40 to 70 times lower than that through an equivalent packed bed of 0.4–0.8 mm beads. This experimental feasibility study has demonstrated that the novel zeolite fibre configuration shows good potential for the production of oxygen-enriched air in a low energy, short cycle time, pressure swing process. The challenges of improving the performance of the adsorbent fibres and their operating parameters are described.

Keywords Low pressure drop structure · Adsorbent hollow fibre · Pressure swing adsorption · Oxygen concentration

J.M. Nevell (✉) · S.P. Perera
Department of Chemical Engineering, University of Bath, Bath, UK
e-mail: ce1jmn@bath.ac.uk

S.P. Perera
e-mail: cessp@bath.ac.uk

1 Introduction

The use of pressure swing adsorption (PSA) to separate air was based on two significant breakthroughs; the development of synthetic zeolites that preferentially adsorb nitrogen over oxygen by Milton (1959a, 1959b) and the invention of efficient pressure swing cycles by both Skarstrom (1960) and Guerin de Montgareuil and Domine (1960). Historically zeolites 5A and 13X have been the most commonly used adsorbents for oxygen concentration. More recently advanced zeolites such as LiLSX have been developed with improved separation performances (Chao 1989). In a standard PSA system zeolite crystals are entrapped with clay binder to form beads used in a packed bed.

Ruthven and Xu (1993) showed that within adsorbent beads sorption kinetics are dominated by macropore diffusional resistance, and that desorption rate is strongly dependent on bead size. For this reason state of the art medical oxygen concentrators such as that invented by Appel et al. (2004) now contain small zeolite beads (such as Zeochem Z12-07 LiLSX beads with a size distribution of 0.4–0.8 mm). Appropriate bead size is related to the bed size, with larger commercial fixed bed PSA devices generally having a bead size larger than 2–3 mm in equivalent diameter (Feng et al. 1998).

Pressure drop is inversely related to the adsorbent bead size (Keller et al. 1987), so any benefit in mass transfer gained through the use of smaller beads is balanced against increased pressure drop. This creates a greater demand on the compressor, needing a larger compressor with a greater energy requirement. A high pressure drop also causes movement of the beads, which results in serious attrition and thus the loss of adsorbent material and plugging of valves and filters in PSA systems.

Li et al. (1998a, 1998b) combated these problems with the development of low pressure drop monolith structures

for air separation by PSA. The pressure drop through the monolith was found to be 3–5 times lower than that through the equivalent packed bed. However the separative performance of the monolith was found to be somewhat inferior to that of the bed of pellets, largely due to its poorer film mass transfer coefficient.

Tai (2007) developed porous hollow fibres containing adsorbent material as a static system for the removal of volatile organic compounds from a vapour stream. The polymer fibres entrap adsorbent particles inside a porous structure and the fibre walls have pore openings in the microfiltration range. Zeolites have been incorporated within hollow fibre membranes since the early 1980s (Caro et al. 2000) with the purpose of producing flawless molecular sieving membranes, however Tai utilised the adsorbent properties of the material rather than using fibres as membranes.

It is intended to develop novel adsorbent hollow fibres for use as a low pressure drop structured adsorbent bed for oxygen concentration. Adsorption occurs via diffusion of air through the structure of the fibre and into the zeolite crystals held inside. The fibre therefore requires a highly open porous structure with low mass transfer resistances. The combination of fast kinetics, a low pressure drop structure and fast pressurisation and depressurisation times will result in an energy efficient PSA system with short cycle times. Fibre columns also provide a stable structure with a longer life due to low attrition. The purpose of this paper is to show the development of these novel adsorbent molecular sieve fibres for oxygen concentration.

2 Experimental

2.1 Materials

The adsorbent hollow fibres were formed using zeolite 13X powder (Zeochem), polyethersulfone (PESF) (Solvay), and 1-methyl-2-pyrrolidone (NMP) (Fluka, ≥98%). Distilled water was used as the internal coagulant and tap water was used as the external coagulant. LiLSX beads (Zeochem Z12-07, 0.4–0.8 mm) and 13X beads (Zeochem ZEOX OII, 0.4–0.8 mm and UOP, 2.0 mm) were used for comparison with fibres. Compressed oxygen (BOC) was used as a purge gas, as required.

2.2 Method

Fibre dope preparation: *general procedure* The desired amount of PESF polymer was weighed out into a wide-neck glass bottle, mixed with the appropriate volume of solvent. The polymer solution was rotated on a roller table until it was fully dispersed and in solution. The solution was stirred under an IKA WERKE bench stirrer at 1000 rev/min and the adsorbent powder was slowly added to the polymer solution. At intervals during this time and afterwards, the stirrer speed was increased to 1200 rev/min to ensure a good dispersion. This is essential in the spinning process, as aggregates can lead to unstable spinning and blocking of the spinneret. The bottle was placed on a roller table for 24–48 hours for degassing. The viscosity of the dope was checked. If it was too viscous, extra solvent was added in 5 g increments and mixed in to achieve ideal spinning viscosity. In order to spin fibres, the viscosity of the polymer solution should generally be between 7–15 Pa s (Tai 2007). For further degassing the dope bottle was placed under vacuum for 30 mins, before being poured into the spinning rig feed vessel. The dope was then left for 30 mins to allow bubbles to rise to the surface before it was ready to be spun.

Spinning adsorbent hollow fibres A schematic diagram of the spinning apparatus is shown in Fig. 1. A double orifice spinneret was used to obtain multi-layer hollow fibres. Single layer fibres were formed by passing dope through only the internal layer. The internal needle size controls the internal diameter of the fibre. A peristaltic pump provided a constant flow of internal coagulant into the bore. It was important to set an appropriate flowrate to create the desired size. The height of the spinneret above the water surface in the coagulation bath was adjusted to achieve the required air gap. The extruded fibre began phase inversion at contact with the water. It was passed through the coagulation bath to further the phase inversion process, and was passed through a second bath for washing before being collected in a water container. The removal rate of fibre from the bath was controlled by a Parvalux motor with a Mitsubishi S500 controller at the end of the rig. This was set to allow the fibre as long as possible in the two baths, while ensuring that the hollow fibre was not subjected to mechanical dragging throughout the spinning process.

Washing, drying and column preparation At the end of the spinning process the manufactured fibre was left in a water container to soak for 3–4 days. This washing step allowed the remaining solvent to migrate out of the fibre, completing the phase inversion. To promote migration of the solvent, the water in the container was frequently changed. Fibre material was air dried, then either formed into a cartridge by straightening, cutting and binding fibres together, or chopped into approximately 10 mm pieces to form a packed bed. Cartridges were sealed on both ends with silicone sealant such that gas could only pass through the bore channels at either end. Zeolite beads are traditionally dried by heating above 250 °C, however this temperature would damage the polymer binder. Instead the fibres were effectively dried by passing heated air at 160 °C through a column containing fibres for 24 hours. This regeneration condition has been confirmed by reproducable results.

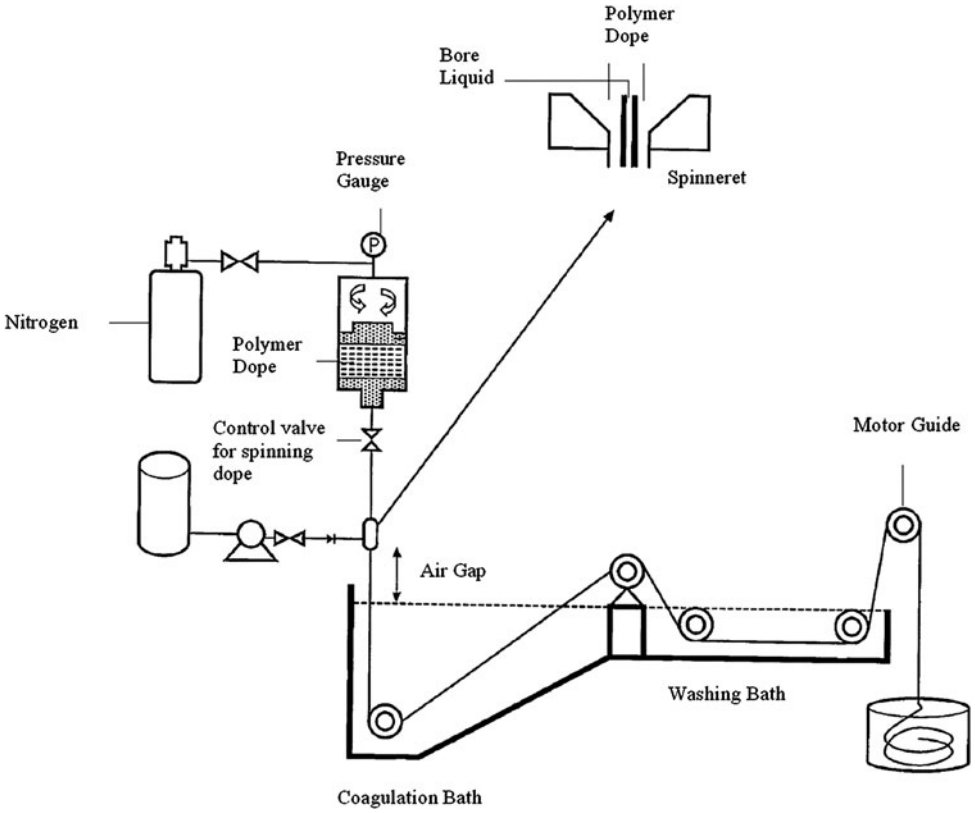

Fig. 1 Schematic diagram of the hollow fibre spinning system (Perera and Tai 2009)

Fibre characterisation by scanning electron microscopy (SEM) Scanning electron micrographs (SEM) were used to characterise the hollow fibre structure and the morphology of the external and bore surfaces, as well as the cross section. Samples were cut with a scalpel blade, then mounted on a specimen plate using a carbon adhesive tab. This was coated with a thin layer of gold in an Edwards S150B Sputter Coater under a vacuum of 0.2 mbara for 4 minutes. The SEM was operated in the 10–20 kV range and micrographs were taken of a number of areas on each sample. Both JEOL JSM6310 and JEOL JSM6480LV microscopes were used for this study.

Oxygen enrichment Figure 2 shows a schematic diagram of the apparatus used for oxygen enrichment experiments. Adsorbent fibres or beads were held inside a stainless steel column (450 mm length, 35 mm internal diameter). This contained perforated metal plates, fine wire meshes and glass wool at both ends to hold adsorbents in place, as well as to prevent fine particles and dust from blocking and damaging the oxygen sensor. Any empty volume after the adsorbent material was added was filled with 3 mm glass beads. Mains compressed air was passed into a buffer vessel via a pretreatment bed of 2 mm 13X beads to remove moisture. Flow to the column was controlled by a Norgren pressure regulator and a Norgren on/off solenoid valve (normally closed). The column could be purged with compressed oxygen, or be evacuated by a Vacuubrand diaphragm vacuum pump. A second solenoid valve allowed depressurization to atmosphere. Huba Control pressure transducers monitored the inlet pressure and the pressure within the column. A Norgren one way valve allowed gas to pass from the top of the column via a Brooks 5850E series mass flow controller to a Teledyne 3010M paramagnetic oxygen analyzer. It was calibrated using pure oxygen and pure nitrogen. A programmable logic controller was used to switch the solenoid valves, and a data logger recorded data from the oxygen analyser and pressure transducers. The oxygen concentration experiments were carried out by passing a steady flow of air through the column at 3 barg feed pressure. The outlet stream was passed at 500 ml/min to the oxygen transducer, before being vented to atmosphere. Experiments were continued until the outlet oxygen composition reached 21%. Pressures and outlet oxygen composition were recorded every second. Experiments were carried out with three different initial conditions prior to the adsorption step:

1. Depressurisation to atmospheric pressure without purge.
2. Bed evacuated for 30 minutes to simulate the vacuum purge step in a VPSA process.
3. Oxygen passed concurrently through the bed at 3 barg and 500 ml/min for 30 min in order to simulate the oxygen purge step of a PSA process.

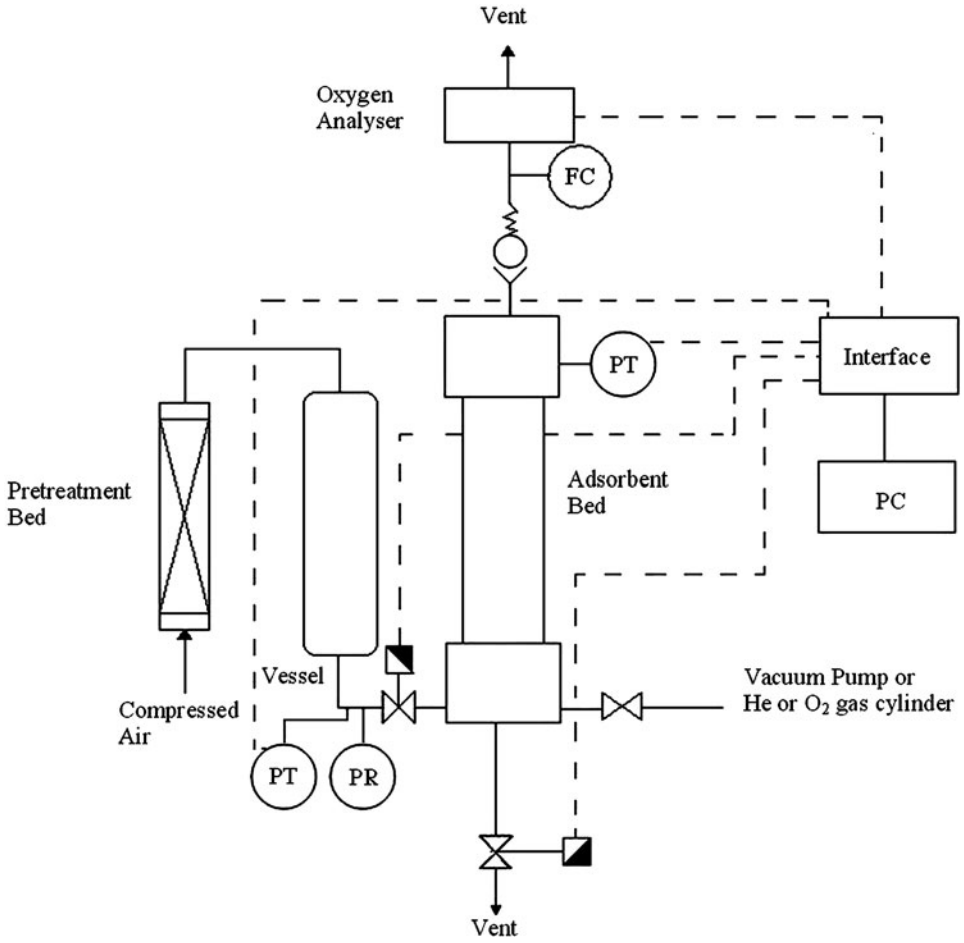

Fig. 2 Schematic diagram of the oxygen enrichment experimental apparatus

Table 1 Summary of the materials tested for pressure drop

Form	Adsorbent material	External diameter (mm)	Internal diameter (mm)	No. fibres
Standard bore fibres	13X	2.2	1	88
Small bore fibres	13X	3	0.54	47
Standard beads	13X	2	–	–
Small beads	LiLSX	0.4–0.8	–	–

Pressure drop A column of 190 mm length and 22 mm internal diameter was fed nitrogen (BOC) at steady flow maintained by a Brooks 5850E series mass flow controller and monitored by a rotameter. Pressure drop measurements were taken using a manometer fitted across the column. The column was filled with fibres or beads as detailed in Table 1. The bed volume was fixed to be the same for all materials tested. Fibres were cut to 190 mm, bound and sealed with silicone to allow gas to pass only through the bore of the fibre. Pressure drops were measured and calculated according to (1), and are presented in Figs. 23 and 24

$$(\rho_{water} - \rho_{nitrogen})gh = \frac{\Delta P}{L'} \tag{1}$$

where ρ is density, g is gravitational acceleration, h is the height of water in the manometer, ΔP is the pressure drop, and L' is the length of the bed.

3 Results and discussion

3.1 Hollow fibre development

Figures 3 and 5–16 show scanning electron micrographs taken of 13X fibres. Figure 3 shows a scanning electron micrograph of an adsorbent hollow fibre, indicating the central bore through which air will flow, and the macrovoids that allow air to permeate radially inside the fibre wall. Within the structure zeolite crystals are held, as can be seen in Fig. 7.

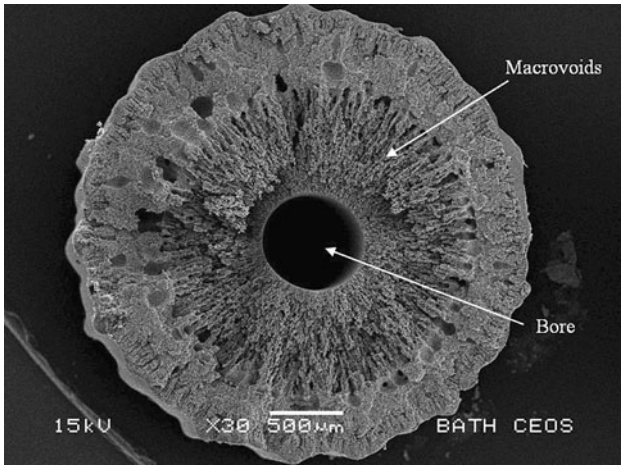

Fig. 3 A scanning electron micrograph indicating the bore channel and the formation of macrovoids within an asymmetric adsorbent hollow fibre containing 13X. ×30

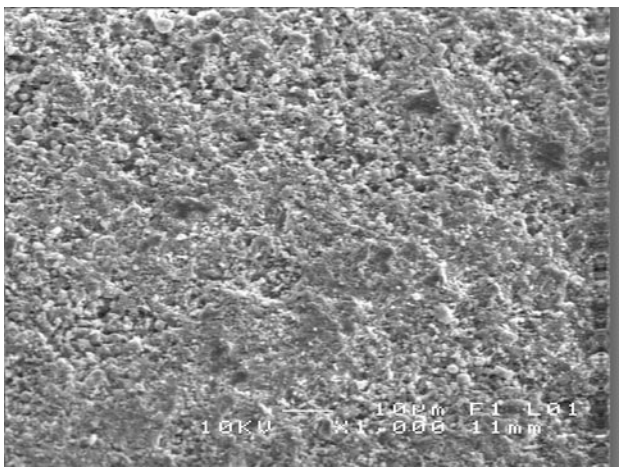

Fig. 4 A scanning electron micrograph of the cross section of a zeolite bead. ×1000

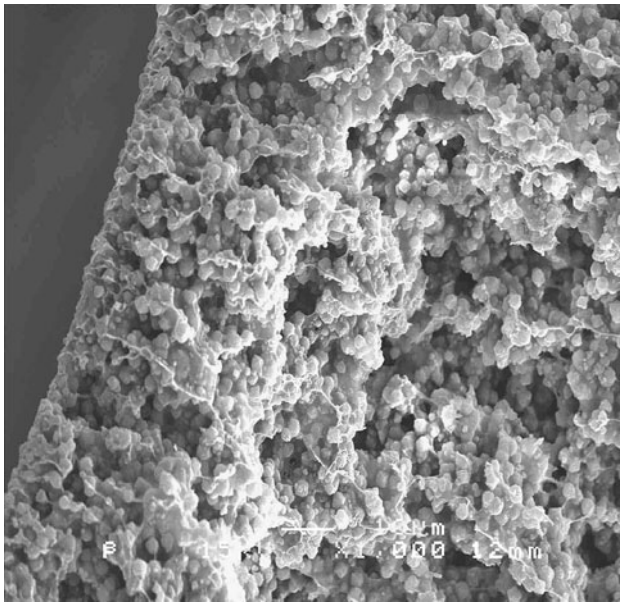

Fig. 5 A scanning electron micrograph of the cross section of a 13X fibre with a polymer:zeolite ratio of 18:82. ×1000

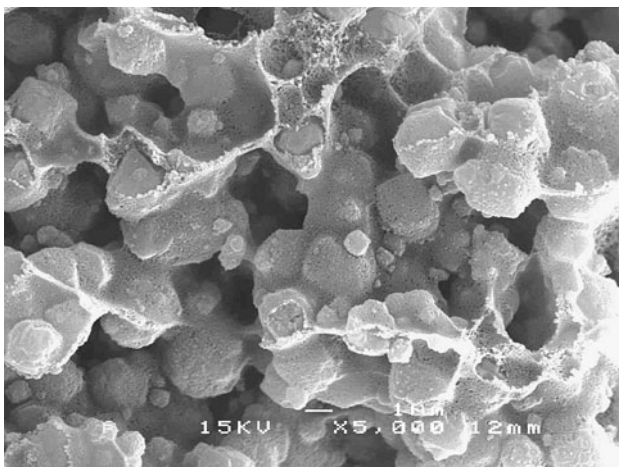

Fig. 6 A scanning electron micrograph of the cross section of a 13X fibre with a polymer:zeolite ratio of 18:82. ×5000

The polymer material acts as a structural support for the adsorbent material, while the macrovoids act as channels through which air can gain access to the zeolite. Figure 4 shows an adsorbent bead in which zeolite crystals are held together with clay binder. This binder creates a high resistance to mass transfer within the bead, slowing access to the adsorbent material. Figures 5 and 6 show fibres with a polymer:zeolite ratio of 18:82. Figure 6 shows many of the zeolite crystals are coated in polymer material, which would impede air access into the adsorbent. In comparison, Figs. 7 and 8 display images of fibres with a polymer:zeolite ratio of 14:86, and Figs. 9 and 10 show a polymer:zeolite ratio of 10:90. Increasing the zeolite loading appears to create more open structures, which provides easier access to the zeolite crystals. Figure 11 shows the cross section of a double layer fibre spun with a standard bore, which was formed by forcing dope through both the inner and outer cavities of the spinneret. Figure 12 shows a single layer fibre with a small bore. Single layer fibres have thinner walls than double layer fibres, meaning a shorter diffusional distance from the bore to the extremities of the fibre. However as shown in Figs. 13 and 14, the external surface of a double layer fibre appears more highly porous than the single layer fibres, which may result in greater overall access to the zeolite material held within the structure. Figures 3, 5 and 11 show a unique ridged external skin that has been created on double layer fibres, which increases the overall external surface area. In comparison, Fig. 12 shows a circular shaped single layer fibre. Figures 15 and 16 show the internal skin when different coagulant fluids are used in the bore.

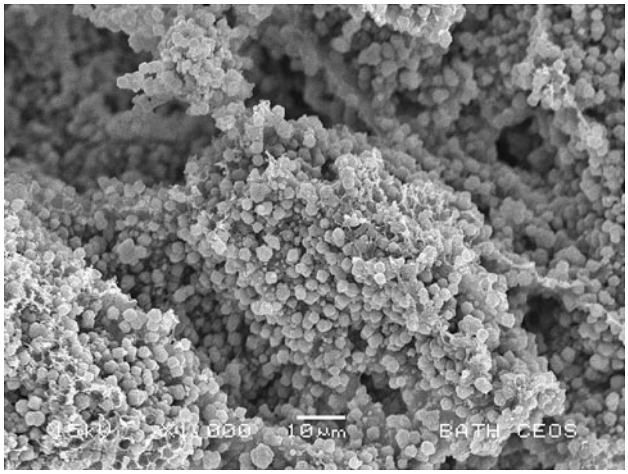

Fig. 7 A scanning electron micrograph of the cross section of a 13X fibre with a polymer:zeolite ratio of 14:86. ×1000

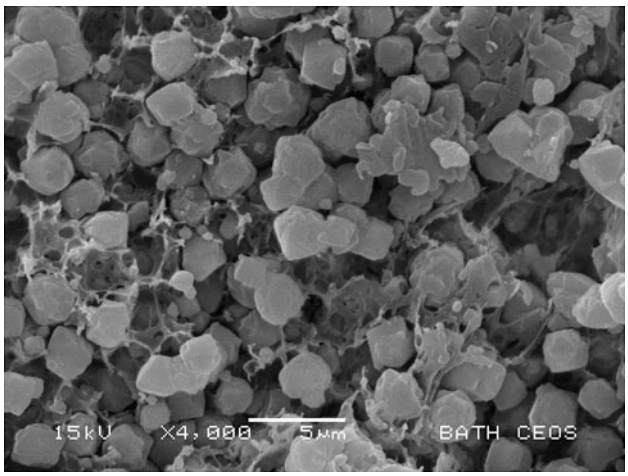

Fig. 8 A scanning electron micrograph of the cross section of a 13X fibre with a polymer:zeolite ratio of 14:86. ×4000

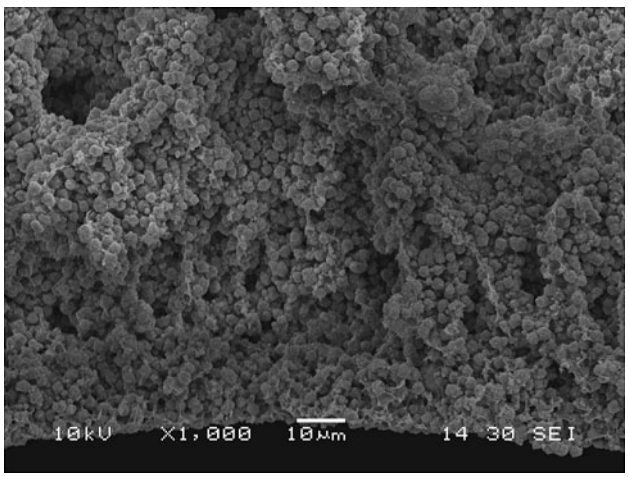

Fig. 9 A scanning electron micrograph of the cross section of a 13X fibre with a polymer:zeolite ratio of 10:90. ×1000

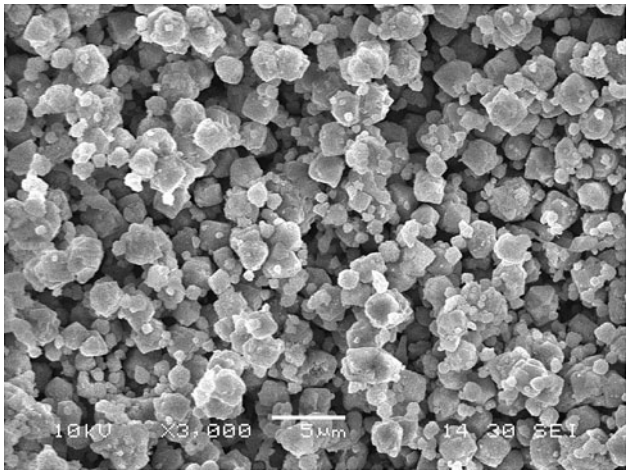

Fig. 10 A scanning electron micrograph of the cross section of a 13X fibre with a polymer:zeolite ratio of 10:90. ×3000

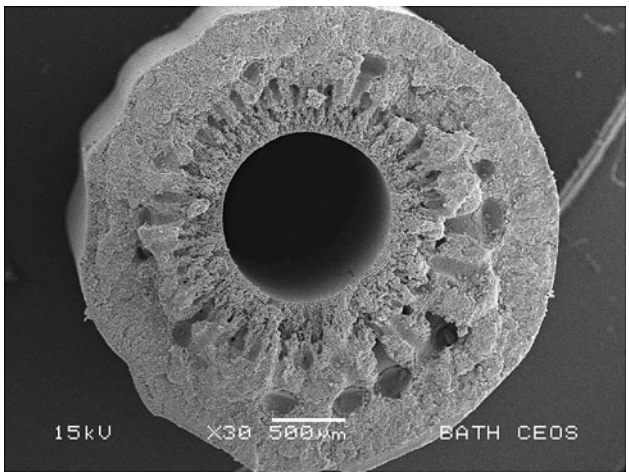

Fig. 11 A scanning electron micrograph of the cross section of a double layer standard bore 13X fibre. ×30

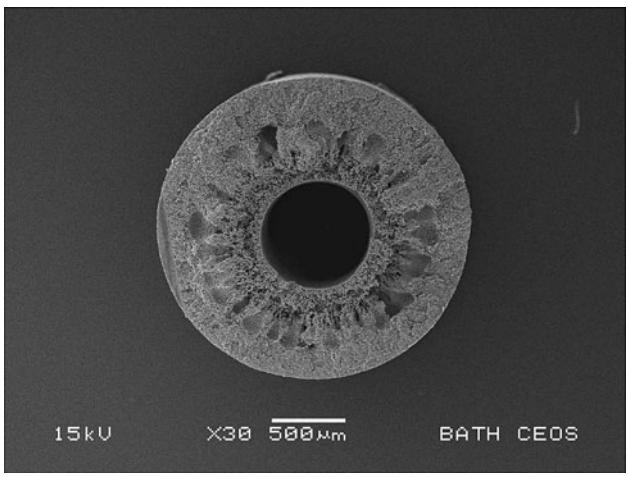

Fig. 12 A scanning electron micrograph of the cross section of a single layer small bore 13X fibre. ×30

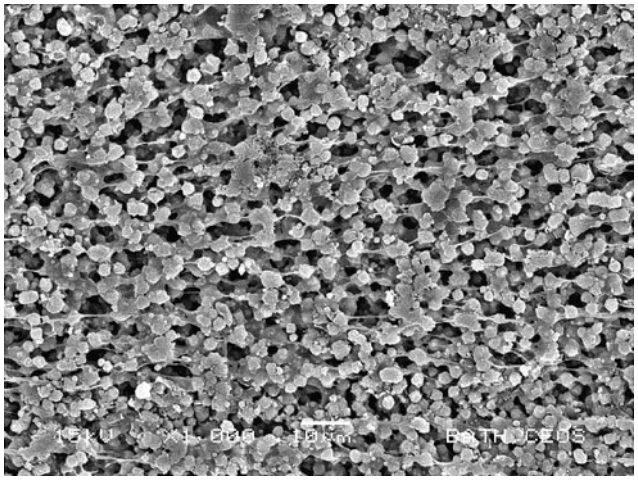

Fig. 13 A scanning electron micrograph of the external surface of a double layer 13X fibre with a polymer:zeolite ratio of 14:86. ×1000

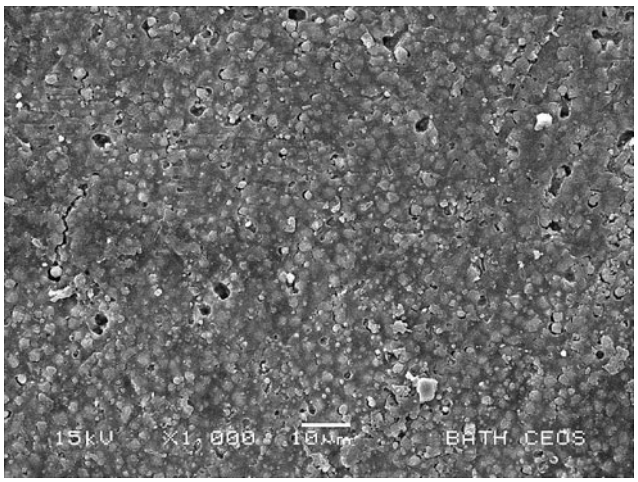

Fig. 14 A scanning electron micrograph of the external surface of a single layer 13X fibre with a polymer:zeolite ratio of 14:86. ×1000

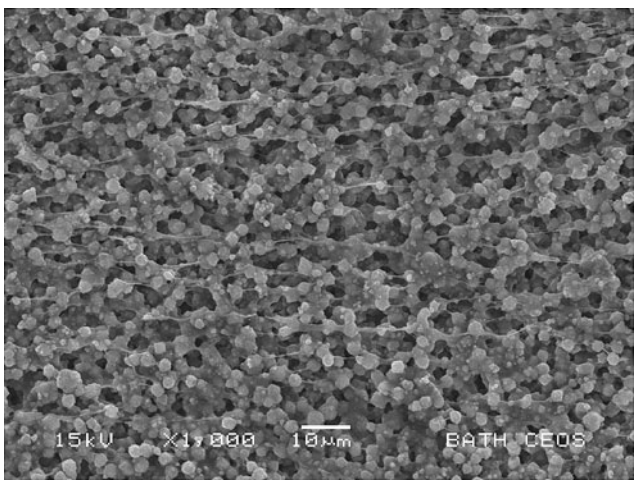

Fig. 15 A scanning electron micrograph of the internal bore surface of a single layer 13X fibre with a polymer:zeolite ratio of 14:86, spun with water internal coagulant. ×1000

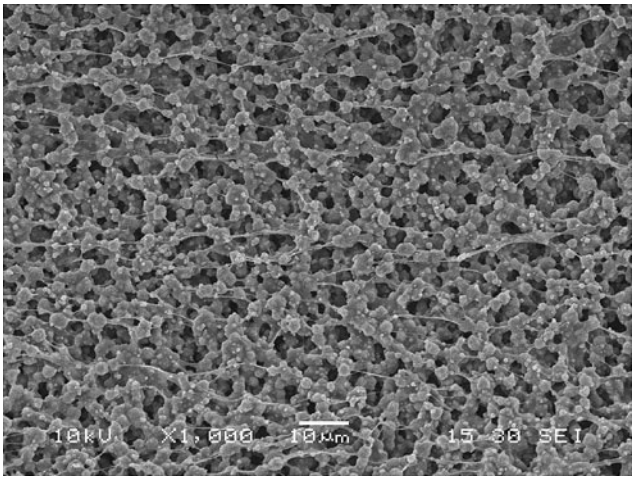

Fig. 16 A scanning electron micrograph of the internal bore surface of a single layer 13X fibre with a polymer:zeolite ratio of 14:86, spun with 50:50 water:NMP internal coagulant. ×1000

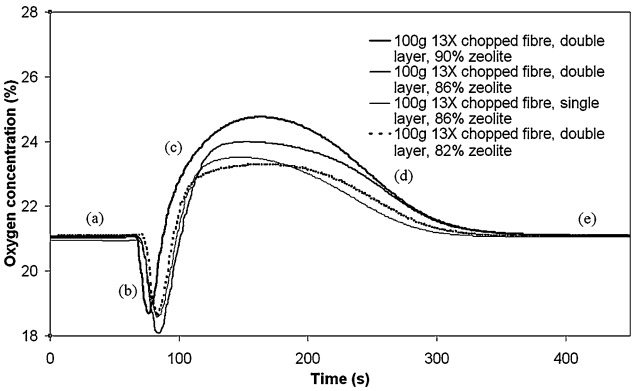

Fig. 17 Temporal profiles of effluent oxygen concentration from 100 g samples of chopped 13X fibres when air passed at 3 barg, 500 ml/min. Column initially depressurized to 0 barg

3.2 Oxygen enrichment

Figure 17 shows the temporal effluent oxygen concentration when passing air at 3 barg through 100 g samples of 13X fibres chopped into roughly 10 mm sections. The column was initially at atmospheric pressure, and no purge has been performed before pressurizing with air. The curves follow the same pattern. In zone (a) indicated on Fig. 17 the concentration remains stable as air in the tube connecting the column to the oxygen analyzer passes through. The oxygen concentration then decreases in zone (b) as previously adsorbed nitrogen is released from the bed. This negative peak does not occur when an effective purge has been performed as the stored nitrogen is either extracted by vacuum or replaced by another gas. In zone (c) the concentration then begins to rise as the less strongly adsorbed oxygen breaks through at the end of the bed, before peaking then decreasing in zone (d) as the adsorbent becomes saturated with nitrogen. When the

Table 2 Estimates of nitrogen loading on adsorbent material and areas under the curves presented within Sect. 3.2

Adsorbent material	Size	Sample mass (g)	Purge	N_2 loading (g)	Area under curve	Figure
90 wt% 13X chopped fibre	Double layer	100	None	0.49	542	17 and 19
86 wt% 13X chopped fibre	Double layer	100	None	0.39	427	17
86 wt% 13X chopped fibre	Single layer	100	None	0.28	312	17 and 22
82 wt% 13X chopped fibre	Double layer	100	None	0.3	326	17
90 wt% 13X chopped fibre	Double layer	100	Vacuum	0.98	1081	18
86 wt% 13X chopped fibre	Double layer	100	Vacuum	0.66	728	18
86 wt% 13X chopped fibre	Single layer	100	Vacuum	0.51	564	18
82 wt% 13X chopped fibre	Double layer	100	Vacuum	0.57	632	18
LiLSX beads	0.4–0.8 mm	100	None	0.47	517	19
13X beads	0.4–0.8 mm	100	None	0.33	367	19
13X beads	2 mm	100	None	0.14	157	19
86 wt% 13X chopped fibre (50:50 water:NMP bore fluid)	Single layer	100	None	0.64	698	22

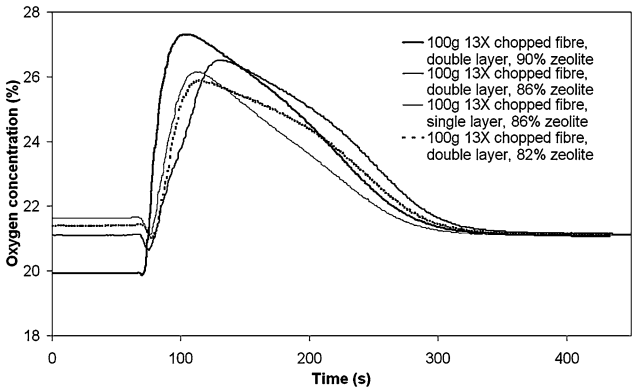

Fig. 18 Temporal profiles of effluent oxygen concentration from 100 g samples of chopped 13X fibres when air passed at 3 barg, 500 ml/min. Column initially evacuated at −0.2 barg for 30 min

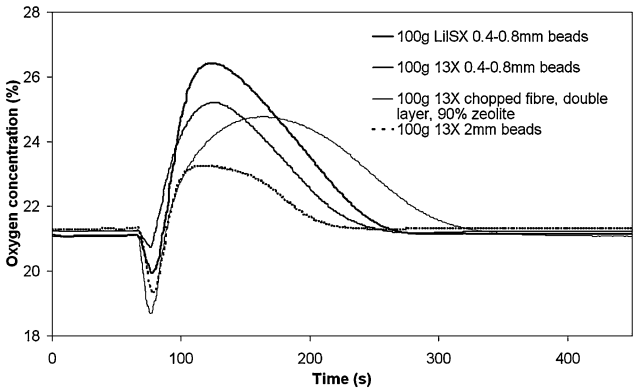

Fig. 19 Temporal profiles of effluent oxygen concentration from 100 g samples of LiLSX and 13X beads, and chopped 13X fibres when air passed at 3 barg, 500 ml/min. Column initially depressurized to 0 barg

bed reaches full saturation the effluent concentration of oxygen becomes equal to that of the feed air, seen as a flat line in zone (e).

The loading of nitrogen into adsorbent material is indicated by the area under the oxygen concentration curve, and an estimate of the loading and the area for each sample can be found in Table 2. The volume of gas adsorbed at each 500 ms interval was estimated by equating input to output in a simple material balance. Loading was then calculated using the ideal gas law, and the area under the curve was estimated using trapezoidal integration.

Figure 18 shows the same experimental conditions as Fig. 17, except the adsorbent bed was evacuated at −0.2 barg for 30 mins before being pressurized with air. It can be seen that the height of the equivalent oxygen peaks is increased by the vacuum purge as the adsorbent initially holds fewer nitrogen molecules within its structure. Figures 17 and 18 compare fibre compositions, showing fibres containing 82, 86 and 90 wt% 13X in PESF. Fibres with a greater proportion of zeolite achieved higher oxygen concentration peaks and increased nitrogen loading. This can be attributed to the improved accessibility of the adsorbent particles due to decreased polymer blocking, as well as the greater density of adsorbent in the structure. These figures also compare samples of single and double layer fibres containing 86 wt% 13X, and show greater nitrogen loadings achieved by double layer fibres. The SEM images in Figs. 13 and 14 indicate that the external surfaces of single layer fibres are less porous than the double layer equivalent, suggesting that more adsorbent material is accessible close to the outer surface of double layer fibres.

Figure 19 compares 90 wt% 13X chopped fibre with 13X beads of both 2 mm and 0.4–0.8 mm diameters. The same experimental conditions as Fig. 17 have been applied. The chopped fibre bed produced an oxygen concentration peak of 24.8%. This is significantly higher than the 23.3% pro-

duced by 2 mm 13X beads, and slightly lower than the peak of 25.2% produced by 0.4–0.8 mm 13X beads. The nitrogen loading on the chopped fibre is 1.5 times greater than that for the 0.4–0.8 mm 13X beads and 3.5 times that for the 2 mm 13X beads. The improved separative performance of the smaller over larger beads is due to the decreased diffusion path length. While a fibre wall thickness of 1 mm gives a diffusion path length inbetween these beads, a thinner fibre may provide better separative performance. Any decrease in diffusion path length must be balanced against losses in mechanical strength in a thinner fibre. The increased nitrogen loading shows that more adsorbent material is accessible in fibres compared with beads. Beads contain approximately 17 wt% binder, so the fibres hold more zeolite. The improved loading on smaller over larger beads suggests that some adsorbent within the structure is blocked by clay binder while fibres with lower binder content are likely to experience less blocking.

Figure 19 also compares the performance of LiLSX zeolite with 13X. 100 g of LiLSX beads produced an oxygen concentration of 26.4%, while the equivalent 13X beads produced an oxygen concentration of 25.2%. This improved separation performance is to be expected since LiLSX has a much higher adsorption capacity for nitrogen than 13X at lower pressures. Zeolites 5A and 13X have historically been the most commonly used adsorbents for oxygen concentration. Through advances in zeolite manufacture, lithium exchanged low silica zeolite X (LiLSX) has been produced. It offers an improvement on the air separation performance due to the smaller shielding electron cloud of the lithium cation (Papai et al. 1995) and the higher density of cations resulting from its low Si/Al ratio (Flanigen 1980). Since LiLSX is currently the best adsorbent material available for oxygen concentration (Gaffney 1996), the incorporation of LiLSX powder within hollow fibres gives scope for future improvements.

A cartridge of 13X hollow fibres made with a double layer structure and 86 wt% zeolite content was fitted to the experimental column. Figure 20 shows the changes in oxygen concentration when air is passed through the 13X fibre cartridge after a 30 minute purge with oxygen at 3 barg. This is compared with the same curve for a bed packed with the equivalent mass of both 2 mm and 0.4–0.8 mm 13X beads. The curve produced by the beads is much sharper than that of the fibres. This indicates that mass transfer into and out of this cartridge of fibres is slower and still needs improving. Figure 21 shows the same experimental conditions performed with 100 g samples of beads, chopped fibres, and the same chopped fibres sliced along the axis. It can be seen that the chopped fibres produce sharper slopes than the straight fibre cartridge. There are several potential reasons for this. Firstly 230 g of fibres completely filled the experimental column, leaving no space at the column ends. Since

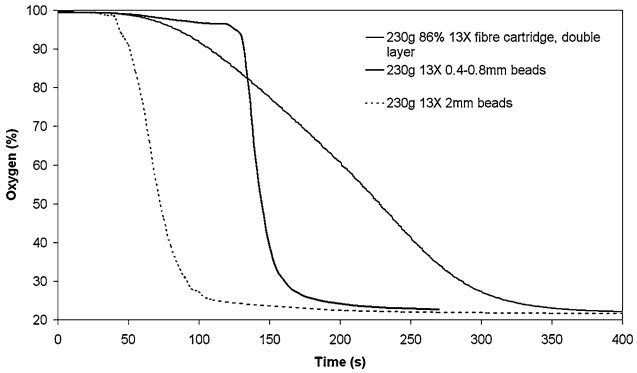

Fig. 20 Temporal profiles of effluent oxygen concentration from a 230 g 13X fibre cartridge and 230 g LiLSX and 13X beads when air passed at 3 barg, 500 ml/min. Column initially purged with oxygen at 3 barg for 30 min

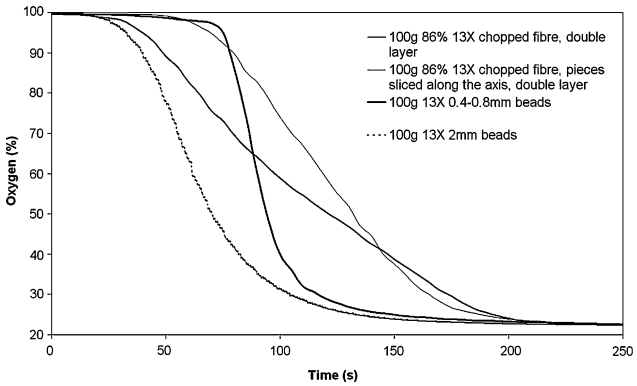

Fig. 21 Temporal profiles of effluent oxygen concentration from 100 g of 13X fibres, the same fibres sliced vertically, and 13X beads when air passed at 3 barg, 500 ml/min. Column initially purged with oxygen at 3 barg for 30 min

the feed tube is of a smaller diameter than the column it is possible that gas flow was unevenly distributed between the fibres, channeling through the central fibres more than the outer fibres. The addition of a conical distributer at either end of the column would ensure an even distribution of gas. Secondly the fibre structure presents resistance to mass transfer. Gilleskie et al. (1995) showed that unlike in conventional beads, adsorbent hollow fibres contain a resistance due to the hollow fibre wall. There is scope for further development of the fibres to create greater porosity and faster kinetics. Thirdly the chopped fibres present a lower macropore resistance because more fibre surface is open to the air. This is confirmed by the sharper slope of the chopped fibres after they have been sliced further.

Figure 22 shows the same experimental conditions as Fig. 17, and compares single layer fibres of the same composition that had been spun using different bore fluids. The fibre spun with 50:50 water:NMP as the bore coagulant showed improved separation performance and nitrogen loading when compared with the fibre spun with water in

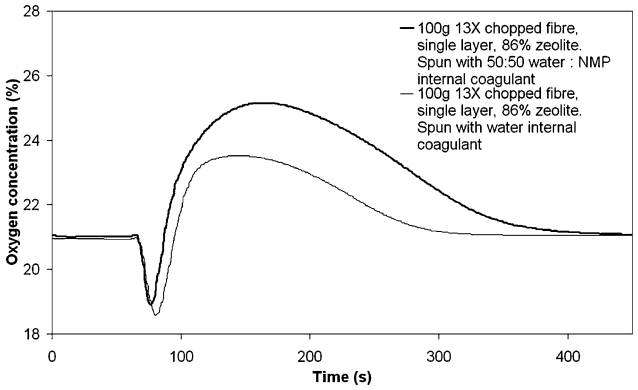

Fig. 22 Temporal profiles of effluent oxygen concentration from 100 g samples of chopped 13X fibres when air passed at 3 barg, 500 ml/min. Column initially depressurized to 0 barg

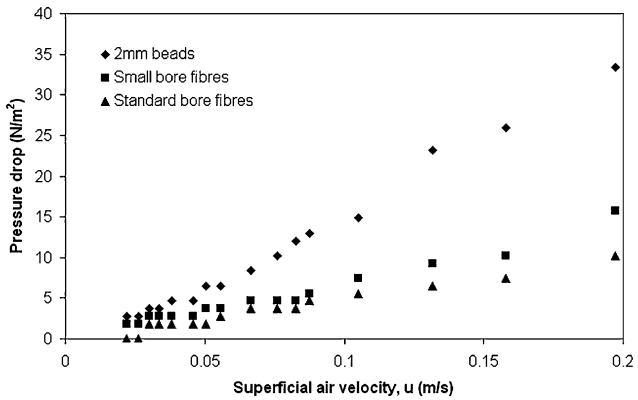

Fig. 23 Comparison of steady flow pressure drops for small and standard bore fibre cartridges and 2 mm standard beads

the bore. When fibre dope comes into contact with water there is an instant solidification at the surface as NMP enters the aqueous phase. The addition of solvent within the bore fluid delays demixing and coagulation on the inside of the fibre, resulting in a more open structure close to the bore. Scanning electron micrographs in Figs. 15 and 16 show the surface of the bore channels in both fibres, however they do not reveal a clear difference in the structure of the skin.

3.3 Pressure drop

Fibres can be spun using different internal needles to vary the bore diameter. Two are considered in this study: small bore (0.54 mm diameter) and standard bore (1 mm diameter). The pressure drops across cartridges made with these fibres are compared with that across a bed of the same volume containing 2 mm beads in Fig. 23, and with 0.4–0.8 mm beads in Fig. 24. In the superficial velocity range 0.02–0.20 m/s the pressure drop across the cartridge of small bore fibres was between 1 and 2 times higher than the standard bore fibres. For the same superficial velocity range, the pressure drop across the 2 mm beads was between 1.5 and

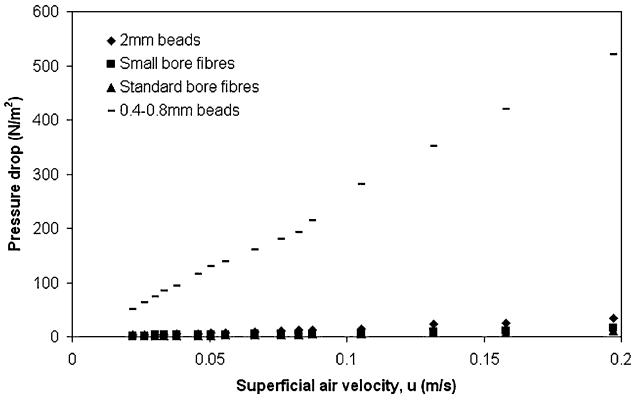

Fig. 24 Comparison of steady flow pressure drops for 0.4–0.8 mm small beads with pressure drops for small and standard bore fibre cartridges and 2 mm standard beads

4 times higher than across the fibres, while across the 0.4–0.8 mm beads it was between 40 and 70 times that of the fibres. The pressure drop advantage of using a larger bore must be balanced against the loss of volume occupied by adsorbent material. Hollow fibres show a clear advantage as low pressure drop structures compared with packed beds of beads. Theoretical pressure drop values (not included here) have been calculated according to (2) (Patton et al. 2004) and (3) (Gilleskie et al. 1995), and follow a similar trend to the experimental data.

$$\frac{\Delta P}{L} = \frac{128 Q \mu}{\pi d^4} \tag{2}$$

$$\Delta P = \frac{\upsilon_o}{\epsilon} \frac{32 \mu}{\pi d^2} \tag{3}$$

where ΔP is the pressure drop, L is the length of the bed, Q is the volumetric flowrate, μ is the gas viscosity, d is the inner diameter of the fibre, υ_o is the superficial velocity in the bed and ϵ is the bore volume per bed volume.

4 Conclusions

Adsorbent hollow fibres have been successfully prepared from 82–90 wt% 13X zeolite powder and 18–10 wt% polymeric binder, and have been shown to concentrate oxygen when used as an adsorbent bed for air separation. The fibres are flexible and can be used in a range of configurations. The molecular sieving adsorbent fibre produced showed improved macroporous structure with low binder content, and macrovoids were formed to allow easy access to gas separation. However results showed that the mass transfer resistance within the macroporous structure needs to be improved. This could be done by reducing the diffusion path length by decreasing the fibre wall thickness. The use of a solvent water mixture as the bore coagulant was shown to

improve separation kinetics by creating more open macroporosity during spinning. The adsorbent fibres with either standard or small bore have been shown to function as a low pressure drop structure, with a pressure drop between 40 and 70 times less than that of a packed bed of 0.4–0.8 mm beads of equivalent mass in the superficial velocity range 0.02–0.20 m/s. These results suggest that not only could the power demand in an adsorptive separation process be reduced if a fibre cartridge were to be used, but that the cycle time could also be reduced, thereby leading to a more compact design. Although not tested in this study, other potential benefits of the fibre bed over a bed packed with pellets include no temperature rise on pressurisation, which should lead to an improved performance during the feed step of a PSA process, and a low attrition resistance which could extend the life of the adsorbent. There is also scope for further development of the fibres through the incorporation of LiLSX adsorbent within the structure.

Acknowledgement Thanks to Wendy Ng for her contribution to the pressure drop measurements.

References

Appel, W.S., Winter, D.P., Sward, B.K., Sugano, M., Salter, E., Bixby, J.A.: Portable oxygen concentration system and method of using the same. U.S. Patent 6,691,702 (2004)

Caro, J., Noack, M., Kölsch, P., Schäfer, R.: Zeolite membranes—state of their development and perspective. Microporous Mesoporous Mater. **38**(1), 3–24 (2000)

Chao, C.C.: Process for separating nitrogen from mixtures thereof with less polar substances. U.S. Patent 4,859,217 (1989)

Feng, X.S., Pan, C.Y., McMinis, C.W., Ivory, J., Ghosh, D.: Hollow-fiber-based adsorbers for gas separation by pressure-swing adsorption. AIChE J. **44**(7), 1555–1562 (1998)

Flanigen, E.M.: Molecular sieve zeolite technology—the first twenty-five years. Pure Appl. Chem. **52**, 2191–2211 (1980)

Gaffney, T.R.: Porous solids for air separation. Curr. Opin. Solid State Mater. Sci. **1**(1), 69–75 (1996)

Gilleskie, G.L., Parker, J.L., Cussler, E.L.: Gas separations in hollow-fiber adsorbers. AIChE J. **41**(6), 1413–1425 (1995)

Guerin de Montgareuil, P., Domine, D.: Process for separating a binary gaseous mixture by adsorption. French Patent 1,223,261 (1960)

Keller, G.E., Anderson, R.A., Yon, C.: Adsorption. In: Rousseau, R.D. (ed.) Handbook of Separation Process Technology, p. 644. Wiley-Interscience, New York (1987)

Li, Y.Y., Perera, S.P., Crittenden, B.D.: Zeolite monoliths for air separation part 1: manufacture and characterization. Chem. Eng. Res. Des. **76**(A8), 921–930 (1998a)

Li, Y.Y., Perera, S.P., Crittenden, B.D.: Zeolite monoliths for air separation part 2: oxygen enrichment, pressure drop and pressurization. Chem. Eng. Res. Des. **76**(A8), 931–941 (1998b)

Milton, R.M.: Molecular sieve adsorbents. U.S. Patent 2,882,243 (1959a)

Milton, R.M.: Molecular sieve adsorbents. U.S. Patent 2,882,244 (1959b)

Papai, I., Goursot, A., Fajula, F., Plee, D., Weber, J.: Modeling of N_2 and O_2 adsorption in zeolites. J. Phys. Chem. **99**(34), 12,925–12,932 (1995)

Patton, A., Crittenden, B.D., Perera, S.P.: Use of the linear driving force approximation to guide the design of monolithic adsorbents. Chem. Eng. Res. Des. **82**(A8), 999–1009 (2004)

Perera, S.P., Tai, C.C.: Hollow fibres. U.S. Patent Application US 2009/0305871 A1 (2009)

Ruthven, D.M., Xu, Z.: Diffusion of oxygen and nitrogen in 5a zeolite crystals and commercial 5a pellets. Chem. Eng. Sci. **48**(18), 3307–3312 (1993)

Skarstrom, C.W.: Method and apparatus for fractionating gaseous mixtures by adsorption. U.S. Patent 2,944,627 (1960)

Tai, C.C.: Novel adsorbent hollow fibres. PhD Thesis, University of Bath (2007)